Basic Array Theory

WOLFGANG H. KUMMER, LIFE FELLOW, IEEE

Invited Paper

This paper outlines basic antenna array theory with major emphasis on pattern analysis and synthesis for periodic linear and planar arrays, phased arrays, and conformal arrays. Extension is made to synthesis techniques which use computer algorithms. These include arbitrary side lobe control, shaped beams, and phase-only null steering. The subjects of random errors and phased array quantization errors are outlined.

I. INTRODUCTION

In this paper the basics of array theory will be discussed; extensions of the topics presented here are given in other papers in this issue as well as in the references. The characteristics of linear, planar, and conformal arrays will be treated here insofar as their patterns, beamwidth, and directivity are concerned.

Linear arrays consist of equally spaced elemental radiators[1] laid out in a straight line, while two-dimensional planar arrays consist of radiators oriented on a geometric grid in a plane. Rectangular arrays may be thought as a set of linear arrays placed next to each other, equally spaced, forming the two-dimensional array. A linear array may also be wrapped around a curved surface, usually a circle or a cylinder. Two-dimensional arrays can be formed by replicating these linear arrays along generatrices of cylinders and cones, or wrapping them on spheres.

Linear, planar, and conformal arrays can be designed with either a fixed main beam, or a scanned beam which is rapidly positioned in space by means of electromechanical or electronically actuated devices connected in the feed lines behind the array radiators. These devices change the phase or time-delay between radiators to produce the required phase progression along the array. Scan can be one- or two-dimensional.

The patterns for linear arrays will be analyzed in terms of the main beam, side lobes, and grating lobes. Graphical and analytical methods, as well as simple examples, will be shown. Two synthesis techniques, the Dolph–Chebyshev and the discrete Taylor will be outlined. Extensions to iterative techniques for pencil and shaped beams will be presented. Random and quantization errors will be taken up; the discussion will then be extended to two-dimensional planar arrays.

Conformal arrays are presented, using circular arrays as an introduction. Characteristics unique to conformal arrays are stated; a conformal array pattern synthesis technique is applied to a conical array as an illustration of the technique.

In this last section of the introduction, the electromagnetic equations that form the basis for the development of the array theory will be given. In these radiation problems, one can think of two regions, the first, around the origin of the coordinates, wherein lie the sources of radiation, and the other, in the field region, where the electric field due to these sources is measured.

From the solution of Maxwell's equations in unbounded space, the radiation field, which can be expressed in terms of magnetic and electric vector potentials, simplifies if the distance between the source and the far-field regions is large ($|\overline{r}| \gg |\overline{r}'|_{\max}$), a condition met in most practical situations [3]. The vectors $\overline{r}$ and $\overline{r}-\overline{r}'$ may then be considered parallel (Fig. 1) and

$$|\overline{r} - \overline{r}'| \rightarrow r - r' \cos \xi. \tag{1}$$

We will talk about discrete elements arrayed in a repetitive grid. The electric field of nth element in an array may be expressed as follows:

$$\overline{E}_n(x, y, z) = \left(e^{-jkr}/r\right)\overline{A}_{e_n}(x', y', z')I_n \exp(jkr'_n \cos \xi_n). \tag{2a}$$

The $\overline{A}_e$ term characterizes the individual element and specifies its behavior in terms of the polarization and the orientation of the electric field. The remaining part of (2a) contains the effect of the amplitude, in terms of the currents I_n, and the phase excitation as observed at the far-field point. The field due to the summation of all the array elements is

$$\overline{E}(x, y, z) = \left(e^{-jkr}/r\right) \sum \overline{A}_{e_n} I_n \exp(jkr'_n \cos \xi_n). \tag{2b}$$

Manuscript received October 1, 1990; revised May 18, 1991.
The author is with W. H. Kummer, Inc., Santa Monica, CA 90405.
IEEE Log Number 9105088.

[1] Only the subject of arrays with periodically spaced elements will be considered. For a discussion of aperiodic arrays, the reader should consult the literature [1], [2].

0018–9219/92$03.00 © 1992 IEEE

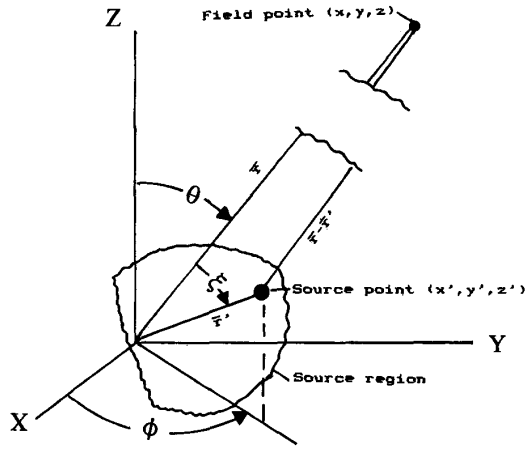

Fig. 1. Geometry for pattern calculations.

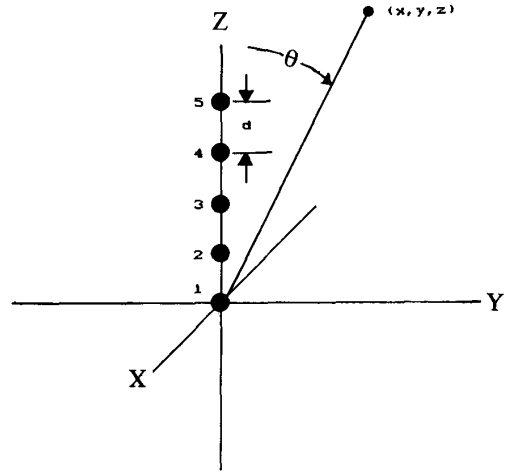

Fig. 2. Linear array coordinate system.

For linear and planar array analysis, the element pattern can be factored[2] from the summation in (2b) [4]. It reads

$$\overline{E}(x,y,z) = \left(e^{-jkr}/r\right)\overline{A}_e \sum I_n \exp(jkr'_n \cos\xi_n) \quad (2c)$$

where A_a, the array factor is given by

$$A_a = \sum I_n \exp(jkr'_n \cos\xi_n). \quad (3)$$

The antenna patterns are plots of the amplitude, and sometimes the phase, of the electric field at a constant distance r; they are normalized, usually to the peak value.

A word about coordinate systems: in the source region, the coordinates most natural for the layout of the sources are used, namely Cartesian, cylindrical, or spherical. Cylindrical or spherical coordinates are used to describe the positions of the field points. A useful relation, in conjunction with (1), is

$$rr' \cos\xi = \overline{r} \cdot \overline{r}' = xx' + yy' + zz'. \quad (4)$$

II. Linear Arrays

A. Pattern Analysis and Synthesis

We postulate a linear array of equally spaced elements, located along the Z axis, with an element spacing of d (Fig. 2). The array factor will have no ϕ variation, only a θ variation; it will be a figure of revolution about the Z axis. The Z axis is chosen for array placement to minimize the number of pattern coordinate variables. Only the array factor will be examined now, later the characteristics of the element will be introduced. From (4): $x' = y' = 0, z' = (n-1)d; z = r\cos\theta$. Equation (3) reduces to

$$A_a = \sum_{n=1}^{N} I_n \exp(j(n-1)kd\cos\theta). \quad (5a)$$

[2]The elements are assumed to be equally spaced, electrically identical and oriented in the same spatial direction.

It is easiest to visualize the pattern behavior with all currents equal, (equal excitation or uniform illumination), namely $I_n = 1$.

$$A_a = \sum_{n=1}^{N} \exp(j(n-1)kd\cos\theta). \quad (5b)$$

At $\theta = 90°$, the exponent becomes zero and all contributions add algebraically; the sum becomes a maximum and equals the peak of the main beam (Fig. 3(a)). This condition will also occur when the exponent $kd\cos\theta = 2\pi$, or multiples thereof, then

$$\cos\theta = \lambda/d. \quad (6)$$

These secondary peaks, called grating lobes, will repeat *ad infinitum* in the array factor as a function of $\cos\theta$. The grating lobes can be excluded from "visible space," which is the range of the angle θ from 0° to 180°, by a proper choice of element spacing, namely, $\lambda/d < 1$. The pattern characteristics of a four-element array will be examined as an example of graphical and mathematical analysis techniques.

To simplify the analysis of the patterns, we let $kd\cos(\theta) = \psi$ in (5b). Think of each phasor $e^{j\psi}$ as a line segment of unit amplitude and phase ψ, in the complex plane. These phasors are added, first with $\psi = 0°$, as in Fig. 3(a), with the resulting maximum of 4. Fig. 3(b) illustrates the summation for $\psi = 30°$; the difference between successive phasors is ψ. The sum will be smaller since the angular difference between successive phasors is 30°. As ψ reaches 90°, a first null is obtained (Fig. 3(c)). Beyond that, the first side lobe is reached around 135°. The next null occurs at 180°, then the pattern repeats in ψ. A plot of the power pattern in decibels is shown in Fig. 4; the nulls are equally spaced in the ψ plane. The corresponding angles are also indicated for two different element spacings, $d/\lambda = 1$ and 1/2, and for two beampointing directions,

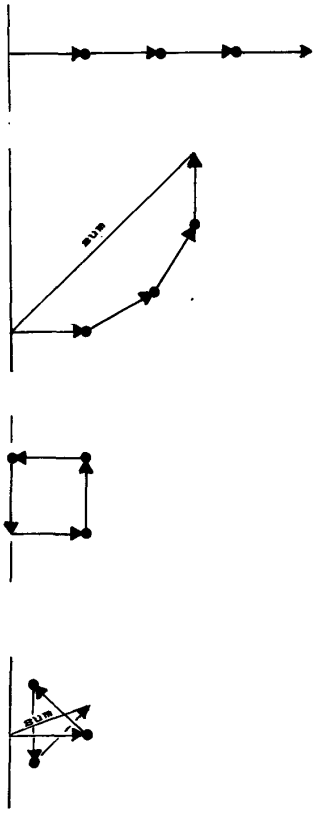

Fig. 3. Phasor presentation of pattern summation. Each phasor is equal to one unit. (a) $\psi = 0°$, sum = 4. (b) $\psi = 30°$, sum = 3.3. (c) $\psi = 90°$, sum = 0. (d) $\psi = 135°$, sum = 1.1.

broadside ($\theta = 90°$) and $\theta = 60°$. For $d/\lambda = 1$, at broadside, a partial grating lobe is evident at $\theta = 0°$ and 180°. For a larger number of elements, the first null would occur at a smaller ψ, thus the null to null , as well as the 3-dB beamwidths would be narrower. If the elements have an amplitude taper distributed symmetrically about the array center, then, compared with uniform illumination, the peak at $\psi = 0°$ is at a lower level, the first null occurs at a larger angle and the first side lobe is lower and also moves out in ψ.[3] This pattern analysis was treated mathematically by Schelkunoff [5], and will be described next.

Schelkunoff makes a further transformation in the angular variable, namely,

$$w = e^{j\psi} \tag{7}$$

and (5a), with the currents normalized, becomes

$$A_a(w) = \sum_{n=1}^{N} \frac{I_n}{I_1} w^{n-1}. \tag{8}$$

[3]An alternate way of examining the behavior of these phasors, by inscribing them and fanning them out in unit circles, has been presented in the literature [4].

Expanded and rearranged it reads [6]:

$$A_a(w) = \left|\frac{I_N}{I_1}\right| \cdot \left|w^{N-1} + \frac{I_{N-1}}{I_N} w^{N-2} + \cdots + \frac{I_1}{I_N}\right|.$$

This polynomial can be written in terms of its roots

$$\begin{aligned} f(w) &= |w - w_1| \cdot |w - w_2| \cdots |w - w_{N-1}| \\ &= \prod_{n=1}^{N-1} |w - w_n|. \end{aligned} \tag{9}$$

We have the new variable w which traverses the circumference of a unit circle (Fig. 5); the product of the terms $|w - w_n|$ gives the pattern amplitudes as a function of w. If we take the uniformly illuminated array, $I_n = 1$,

$$f(w) = \sum_{n=1}^{N} w^{n-1}$$

which can be rewritten, noting that it is a geometric progression:

$$f(w) = \frac{1 - w^N}{1 - w} \tag{10}$$

and the roots occur at

$$w_p = e^{j2\pi p/N}, \qquad p = 1, \cdots, N-1.$$

The magnitude of the pattern may be written $|\sin N(\psi/2)/\sin(\psi/2)|$ with $u = (d/\lambda)\cos\theta$ it becomes

$$\left|\frac{\sin N\pi u}{\sin \pi u}\right|. \tag{11}$$

For the four-element array, $N = 4$, the roots are at $\psi = 90°$, 180°, and 270°. The function $f(w)$, in conjunction with (7), was used to plot the pattern as shown in Fig. 4. The unit circle can be used equally well for a tapered distribution. By moving the roots toward $\psi = 180°$, the side lobe levels will be lowered and the main beam will be broadened. By trial and error, the roots can be adjusted until the desired side lobe levels are obtained. A substitution of the newly found roots into (9) and a multiplication of the terms will give the polynomial of (8). The coefficients of the polynomial correspond to the values of the relative currents. It is clear that this process can be mechanized on a computer and iterated. The purpose here was to give familiarity with the underlying mathematics and the connections between the amplitude taper, the placement of the roots, and the side lobe levels.

To effect beam scanning, by moving the main beam from $\theta = 90°$, a phase progression, α, is introduced between adjacent elements, so that $I_n = I_{on}e^{-j\alpha(n-1)}$. Substituting this new expression for the currents into (5a), we obtain

$$A_a = \sum_{n=1}^{N} I_{0n} \exp(j(n-1)[kd\cos\theta - \alpha]) \tag{12}$$

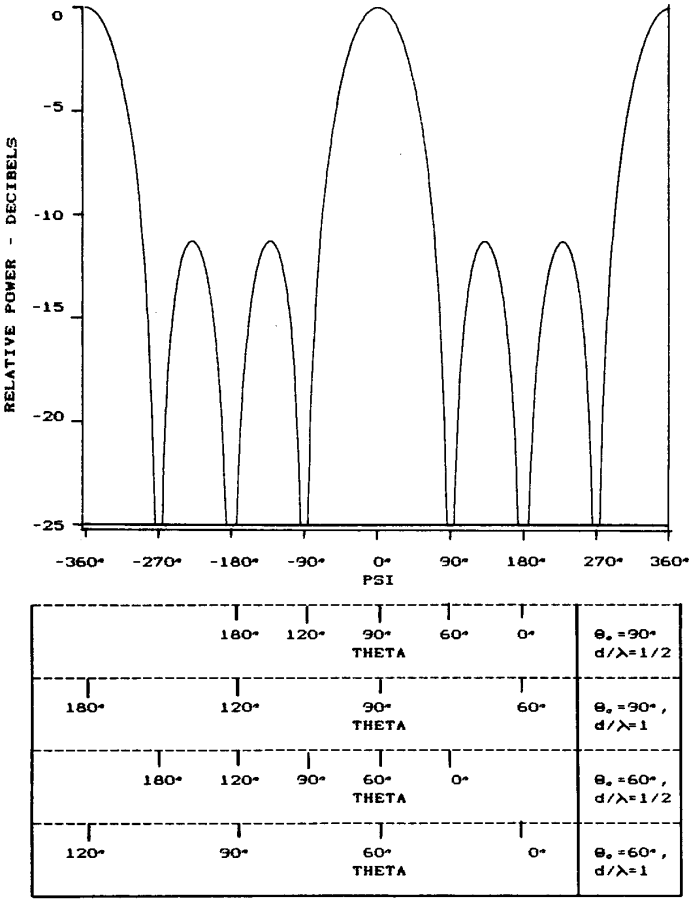

Fig. 4. Array factor of four element uniformly excited linear array.

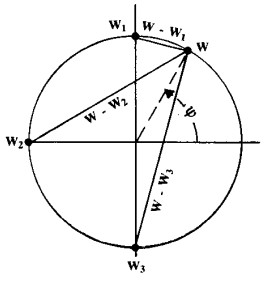

Fig. 5. Schelkunoff unit circle-four element array.

At the peak of the main beam, $\theta = \theta_0$, and the exponent in (12) equals zero, thus $\alpha = kd\cos\theta_0$, and (5a) can be rewritten:

$$A_a = \sum_{n=1}^{N} I_{0n}\exp(j(n-1)[kd(\cos\theta - \cos\theta_0)])$$

then $\psi = kd[\cos(\theta) - \cos(\theta_0)]$. It can be shown, that in order to avoid grating lobes, the condition for a scanned beam becomes

$$d/\lambda \leq \frac{1}{1 + |\cos\theta_0|}. \tag{13}$$

Now let us introduce the element pattern and its role in suppressing the grating lobes. The radiating element chosen for many arrays has a pattern of the form $\sin(\theta)$ which, when multiplied with the array factor (5a), does suppress the peak of the grating lobes, at $\theta = 0°$ and $180°$ for a broadside main beam with an element spacing of one wavelength. However the grating lobes are not completely suppressed, especially for small arrays; also the deep null in the element pattern may not be realized in practice. A more conservative spacing, such as $d/\lambda = 0.7$, may be used to avoid the problem. In scanned arrays, the spacing is reduced to about $d = 0.5\lambda$.

The uniformly illuminated array has a side lobe structure which decreases monotonically from the main beam, with a

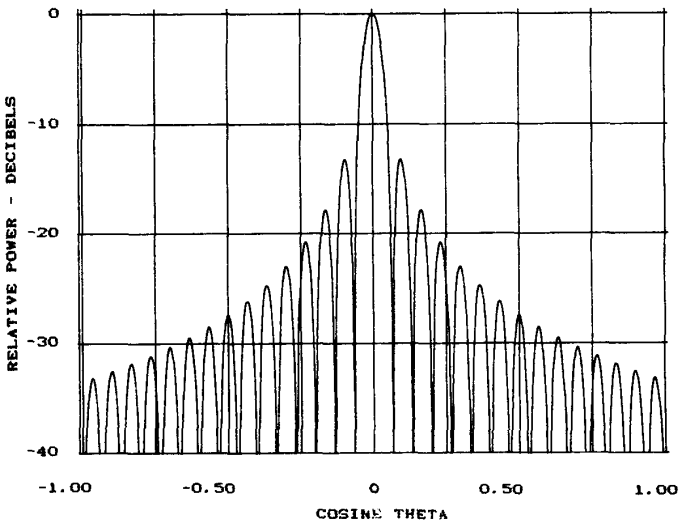

Fig. 6. Pattern of uniformly illuminated array.

first side lobe around 13 dB as shown in Fig. 6. For many applications, lower near-in side lobes are desired. C. L. Dolph [7] addressed that problem by noting the behavior of the Chebyshev polynomials and devising suitable transformations of variables to link the behavior of the polynomials to array side lobe levels. Chebyshev polynomials oscillate between ± 1 for $-1 \leq u \leq 1$ (the inner region) and then increase in absolute value outside the oscillatory region. Figure 7 shows the polynomial of order 4. The oscillations represent the equal side lobe region; the outside region is the main beam. The polynomial can be written, for an odd number of elements [8],

$$\begin{aligned} T_{2N}(u) &= \cos(2N \arccos u), \qquad -1 \leq u \leq 1 \\ &= \cosh(2N \operatorname{arccosh} u), \qquad u \geq 1. \end{aligned} \tag{14}$$

for $(2N+1)$ elements, where the order of the polynomial is $2N$. Transformation of variables is as follows:

$$\psi = kd(\cos\theta - \cos\theta_0)$$
$$u = \cos(\psi/2)$$
$$|\text{sidelobe level}|\text{in dB.} = 20\log\eta, \qquad T_{2N}(u_0) = \eta.$$

The polynomial can also be written in terms of the product of its roots:

$$T_{2N}(u) = cf(w) = \prod_{p=1}^{N}(w - w_p)$$

where c is a constant and the roots are given by

$$\cos(\psi_p/2) = (1/u_0)(\cos(2p-1)\pi/4N), \qquad p = 1, \cdots, 2N.$$

With a symmetrical amplitude distribution, roots occur in complex conjugate pairs, so that the pattern becomes, after some manipulations,

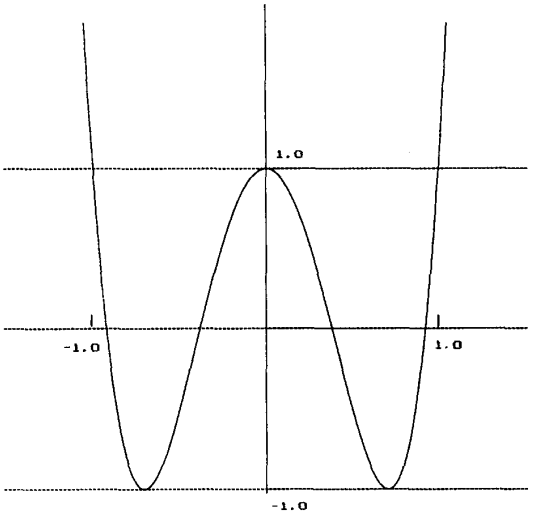

Fig. 7. Chebyshev polynomial of order four.

$$f(w) = w^N 4^N \prod_{p=1}^{N} \sin\left(\frac{\psi - \psi_p}{2}\right) \sin\left(\frac{\psi + \psi_p}{2}\right) \tag{15}$$

which is the Chebyshev pattern for $2N+1$ elements. This distribution is not used in present day pattern designs because the ratio of outer to center currents is high and thus difficult to implement and it does not have low far-out side lobes. However, it is the starting point for the derivation of the Taylor distribution, which will be taken up next.

The Taylor distribution [9] has been the major focus of closed form synthesis techniques. Taylor postulated a pattern from a uniformly illuminated array (with the decreasing side lobe levels) but modified to give equal

close-in lowered side lobes. The technique is a melding of the two, uniform and Chebyshev. Taylor's design was for continuous apertures, wherein the excitation is continuous across the aperture, while we are concerned with discrete elements. Villeneuve has developed the technique for the latter case which obviates the discretization of the continuous distribution [8]. The pattern is written for the uniformly illuminated array; the first $\bar{n}$ roots, of the array factor of the uniform distribution, are replaced with those of the corresponding modified roots of the Dolph–Chebyshev distribution.

$$f(w) = \exp(jN\psi/2)\left(\frac{\sin((2N+1)/2)\psi}{\sin(\psi/2)}\right) \left(\frac{\prod_{n=1}^{\bar{n}-1} \sin((\psi-\psi'_n)/2)\sin((\psi+\psi'_n)/2)}{\prod_{n=1}^{\bar{n}-1} \sin((\psi-\psi'_{0n})/2)\sin((\psi+\psi'_{0n})/2)}\right) \quad (16)$$

The second factor of (16) is the pattern for the uniform distribution, it is multiplied by a fraction: in the numerator are the modified Chebyshev roots for the first $\bar{n}$ close-in side lobes, and in the denominator are the roots corresponding to the uniform distribution for the same $\bar{n}$ roots. Thus the resulting pattern has approximately equal heights for the first $\bar{n}$ roots. The modified Chebyshev roots are used to prevent a sudden jump in the roots at $n = \bar{n}$. They are shifted progressively so that the nth zero coincides with that of the $\sin(2N+1)(\psi/2)/\sin(\psi/2)$ pattern at $\bar{n}$. To accomplish this shift, each Chebyshev zero is multiplied by $\sigma \equiv (\bar{n}\cdot 2\pi)/((2N+1)\psi_{\bar{n}})$, $\psi'_{\bar{n}} = \sigma\psi_{\bar{n}}$, and $\psi_{\bar{n}}$ is the Chebyshev root. An example for a 21-element array with $n = 6$ and 20-dB side lobe levels is shown in Fig. 8.

Other distributions have been developed, several based on Taylor [10]. The usefulness of a particular technique depends on matching system requirements against physically realizable side lobe level distributions, main beamwidth, and gain. These in turn depend on the constraints of array architecture, fabrication, cost, and the resulting unavoidable phase and amplitude errors.

B. Directivity and Beamwidth

For linear arrays, the general equation for directivity, with half-wavelength spaced isotropic elements reduces to [6]

$$D = \left(\sum I_n\right)^2 \Big/ \left(\sum I_n^2\right) \quad (17)$$

where D is the directivity. It shows the basis for antenna directivity and gain, namely, it is proportional to the square of the coherent addition of the currents (phasor addition) divided by the summation of the powers. Also, due to the nature of the conical beams, the directivity is independent of the scan angle. The main beam (in θ) broadens as it is scanned from broadside, while the solid angle occupied by the main beam decreases, just cancelling the widening of the main beam.[4]

[4]For element spacings between $\lambda/2$ and λ, for a constant array length L, the directivity is substantially constant for up to several beamwidths away from broadside. A more general expression may be found in [11].

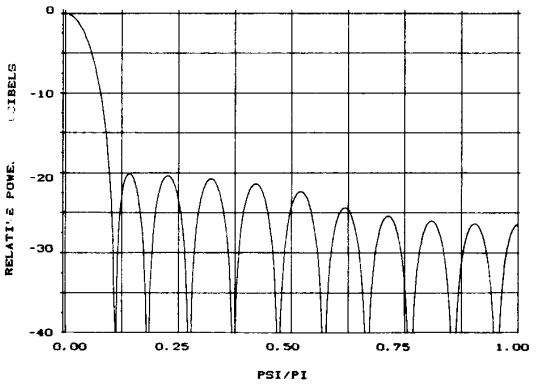

Fig. 8. Computed pattern of discretized Taylor pattern $\bar{n} = 6$, side lobe level 20 dB, $2N + 1 = 21$ (from Villeneuve [8]).

Expressions have been developed for the directivity and beamwidth of uniformly illuminated arrays. One such expression for directivity is $D = 2L/\lambda$, where the array length $L = Nd$, and $(L \gg \lambda)$. For beams around broadside, it is equal to $0.886\lambda/[L\sin(\theta_0)]$. The relationship between directivity D and beamwidth at broadside is $D = 101.5/$ beamwidth, where the beamwidth is expressed in degrees. Corresponding expressions are available for Dolph–Chebyshev distributions [6].

III. Two-Dimensional Arrays

Simple two-dimensional rectangular arrays are composed of linear arrays arranged side by side. The subject of pattern analysis will be examined first. The convention is to locate the array in the XY plane, with the broadside direction along the $+Z$ axis (Fig. 9). The inputs to (4) take the following form:

$$x' = md_x,\ y' = ndy,\ z' = 0;$$
$$x = r\sin\theta\cos\phi,\ y = r\sin\theta\sin\phi.$$

The general pattern for a broadside beam is

$$A_a(\theta,\phi) = \sum_{m=-M}^{M}\sum_{n=-N}^{N} I_{mn}\exp\,(jk \cdot \sin\theta(md_x\cos\phi + nd_y\sin\phi)). \quad (18)$$

where d_x and d_y are the interelement spacings in the x' and y' directions, respectively.

While the excitation of the elements is at the command of the designer, the overall design is constrained by feed complexity and cost. Thus many practical designs use identical feeds that sum one row of radiating elements at a time (thus creating a linear array), the outputs of all linear arrays are then connected by a feeding network. This reduces feed complexity, volume, and cost, but restricts the available array amplitude distributions, and side lobe control. The array factor for such a separable distribution,

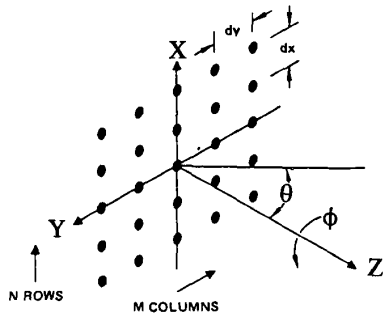

Fig. 9. Planar array coordinate system.

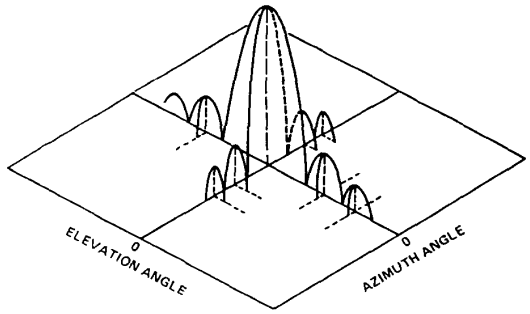

Fig. 10. Planar array pattern-separable distribution.

as it is called, may be written as follows:

$$A_a(\theta,\phi) = \left(\sum_{-M}^{M} I_m \exp(jmkd_x \sin\theta\cos\phi)\right) \cdot \left(\sum_{-N}^{N} I_n \exp(jnkd_y \sin\theta\sin\phi)\right). \quad (19)$$

We have the product of two linear array factors. The patterns along the principal planes are those of the corresponding linear array distributions, while, in the intercardinal planes, they are the products of the two. Figure 10 shows a typical pattern. One of the limitations of separable distributions is higher side lobes along the principal planes and much lower ones elsewhere. Synthesis techniques for linear arrays may be used separately for both axes. For the nonseparable case, other synthesis techniques are available. For rectangular arrays, the Tseng–Cheng distributions are analogous to the Dolph–Chebyshev [12]. The characteristics of two-dimensional scanned arrays with separable distributions will be examined in the next few paragraphs.

The equation for a scanned beam with a separable distribution is

$$A_a = \left(\sum_{-M}^{M} I_m \exp(jm(kd_x \sin\theta\cos\phi - \alpha_x))\right) \cdot \left(\sum_{-N}^{N} I_n \exp(jn(kd_y \sin\theta\sin\phi - \alpha_y))\right) \quad (20)$$

where $\alpha_x = kd_x \sin\theta_0 \cos_0$ and $\alpha_y = kd_y \sin\theta_0 \sin\phi_0$. The beam due to the array summed along the X axis will be a cone rotationally symmetric about the X axis, while the beam from the elements arranged parallel to the Y axis will be symmetric about the Y axis. The following condition must be met for these two beams to form a pencil beam [4], $(\alpha_x/kd_x)^2 + (\alpha_y/kd_y)^2 \leq 1$. The confluence of these two beams at, say the -3-dB contour, gives a pencil beam contour which changes with scan angle as shown in Fig. 11.

The areal beamwidth, that is, the area of the 3-dB beamwidth contour expressed in degrees squared, is [6]

$$B = |\Theta_{x0}\Theta_{y0}|/\cos\theta\cos\theta_0$$

where B is the beamwidth, Θ_{x0} is the broadside beamwidth of the X-directed cut of the beam; Θ_{y0} is the corresponding

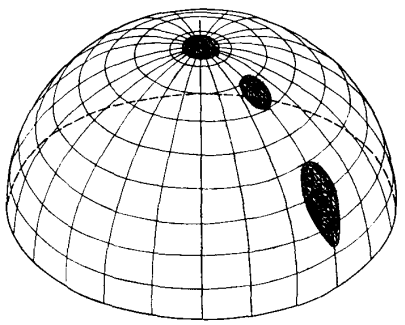

Fig. 11. Beam broadening with scan angle (from Von Aulock [14]).

one for the Y-cut. There is beam broadening as one departs from the broadside direction. One can think of this as resulting from a decrease in the projected area, the area in the direction perpendicular to the beam pointing direction.

The directivity for a uniformly excited array is $D = 4\pi A\lambda^2$ where A is the projected area. The directivity decreases for arrays consisting of discrete elements and further depends on the aperture illumination [6]. The beamwidth and the directivity are related by the approximate expression $D = 32400/B$, where B is the areal beamwidth in square degrees.

As was the case with linear arrays, lattice spacing will determine the onset of grating lobes.[5] In the principal planes (13) applies

$$(d_{x,y}/\lambda) \leq 1/(1 + |\sin\theta_{0_{x,y}}|) \quad (21)$$

where $\theta_{0_{x,y}}$ is the maximum scan angle in the x and y planes, respectively. In other directions, the relations are more complicated [14].

While the previous analysis was applied to rectangular lattices, other lattices are also used in practice. The type of configuration of the elements in the array, the array lattice, is related to the number of radiating elements and phase

[5] Mutual coupling between elements must be taken into account in the design of the array. As the array is scanned from broadside, effects, such as mismatch and blind spots can occur; these are not taken into account by the analysis outlined here. For more on this subject, the reader should consult the literature [13].

shifters required in a phased array for a given beam scan, before the onset of grating lobes. It has led to different element lattices; both rectangular and triangular lattices have been employed, Fig. 12, with the triangular lattice using 15% fewer elements for the same scan limits [15].

IV. Array Errors

The theoretical patterns of the linear and planar arrays, discussed so far, have exhibited infinitely deep nulls and perfect symmetry. Practical arrays have errors due to fabrication tolerances as well as position and orientation errors of the radiating elements. Some of the errors may be systematic due to say, array bending, feed network architecture [16], and phase shifter quantization, others will be random. We will examine random errors first.

A look at the phasor diagrams of Fig. 3 shows the effects of random errors in a qualitative way. Small errors in the length and angle between phasors will raise the null depths; the peak of the main beam will be lowered as well. These random errors will appear in the amplitude and phase terms of a linear array pattern as follows:

$$A_a = \sum I_n(1 + \Delta_n)\exp(j(n\psi + \delta_n)) \qquad (22)$$

where Δ_n and δ_n the amplitude and phase errors of the nth element, respectively. If the errors are independent, and are normally distributed with zero mean, the expected value of the power pattern A_a^2 becomes [17]

$$A_a^2 = A_0^2 + \frac{\sigma^2}{D}$$

where A_0^2 is the error-free power pattern, D is the directivity, and σ is the variance; $\sigma^2 = \sigma_\Delta^2 + \sigma_\delta^2$. The probability of side lobes exceeding a stated level has been examined by Hansen [17]. Figure 13 shows this probability for a 20-element array with uniform excitation.

A. Quantization Errors in Phased Arrays

Phase shifters used in the present-day phased arrays are most often digital devices or analog devices which are digitally controlled [18]. The phase is quantized, instead of being continuously variable and giving the required phase at each element. The smallest phase increment, in degrees, is $360°/2^P$, where P is the number of bits. The peak phase error is $\pm(180°/2^P)$.

For a two-bit phase shifter the available phase states are 0°, 90°, 180°, 270°, (360°); the peak error is ±45°. As seen in Fig. 14, there will be a staircase phase progression across the array [19]. For example, think of two adjacent elements in the array, and suppose that they require phase settings of 67.5° and 112.5°, the two bit-phase shifter for these elements will be set to 90°. Pairs of elements will have the same phase and act like one entity, or a subarray. If the element spacing is $\lambda/2$, then these pairs are λ apart. One can imagine that the array structure broken up into two arrays, each consisting of elements spaced one wavelength apart; as the array is scanned from broadside, quantization grating lobes will appear. In order to reduce these lobes, the

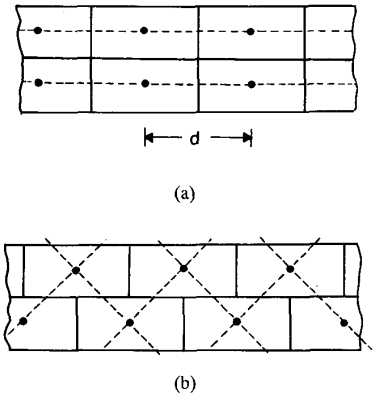

Fig. 12. Lattice layout for phased arrays. (a) Rectangular. (b) Triangular.

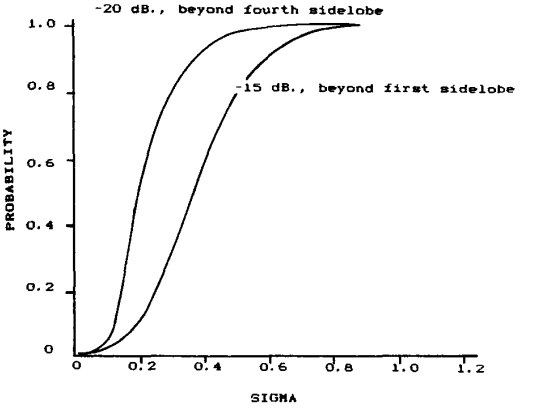

Fig. 13. Probability of side lobes above-stated level uniform distribution, 20 elements (from Hansen [17]).

phase quantization errors are decorrelated by introducing small errors into the array feed network, or by the addition of an extra phase bit. A parabolic phase taper may also incorporated in the feed.

The staircase phase progression causes an array gain loss which is approximately [20]:

$$(\Delta G/G_0) = \pi^2/(3 \times 2^{2P}). \qquad (23)$$

For $P = 3$, the loss is 0.23 dB. Peak quantization side lobes are given, for small scan angles, by $\approx 1/2^{2P}$. For $P = 3$ the peak quantization lobe is −18 dB; for $P = 4$, it becomes −24 dB. The root mean square (rms) side lobe level is $5/(N2^{2P})$ where N is the number of elements. For $N = 100$, with $P = 3$, the rms side lobe is −31 dB.

In most cases, with proper phase dispersion incorporated in the array, 3- or 4-bit phase shifters are adequate; for low side lobe designs, 5 bit may be needed. There may also be amplitude quantization due to phase shifter loss variations with phase state. During design trade-offs, both amplitude and phase errors are incorporated into the pattern computations.

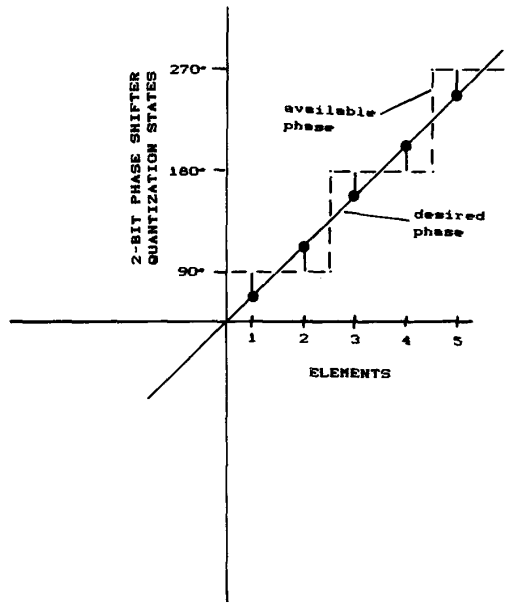

Fig. 14. Phase quantizations for 2-bit phase shifter.

V. Pattern Optimization

The closed-form classical techniques have been used as the basis for pattern designs using computer algorithms that allow greater freedom in array design. As pointed out previously, pattern synthesis involves the positioning of the roots of polynomials to get the desired side lobe control or pattern shape. First, pencil beams with arbitrary side lobe levels will be discussed.

To obtain arbitrary side lobe control, Elliott [21] has generalized the analysis so that the roots of the polynomial can be positioned to control individual side lobe heights on both sides of the main beam; only a few iterations are needed. An example of such a design uses a 19-element slot array with the theoretical pattern shown in Fig. 15(a); the corresponding pattern for an X band experimental array is shown in Fig. 15(b) [22]. As can be seen, good agreement between experiment and theory was obtained. Next, a brief look will be taken at the synthesis of shaping arbitrary beams.

For many requirements, beamshapes with arbitrary contours are needed. One well known method to achieve such requirements is that due to Woodward [23]. He uses linear arrays with uniform amplitudes and linear progressive phase distributions as the building blocks. These arrays have beams, each of which is scanned to a different angle theta, and are so positioned that the peak of each beam falls on the nulls of all the other beams; these beams are thus orthogonal in space. The peak of each beam is adjusted to coincide with the desired shaped beam at the sample points (Fig. 16). The pattern of each beam may be written (see [11]), $a_n[\sin N\pi(u-n)]/N\sin\pi(u-n)$, where a_n is the peak amplitude of the nth beam, and $u = (d/\lambda)(\cos\theta - \cos\theta_0)$.

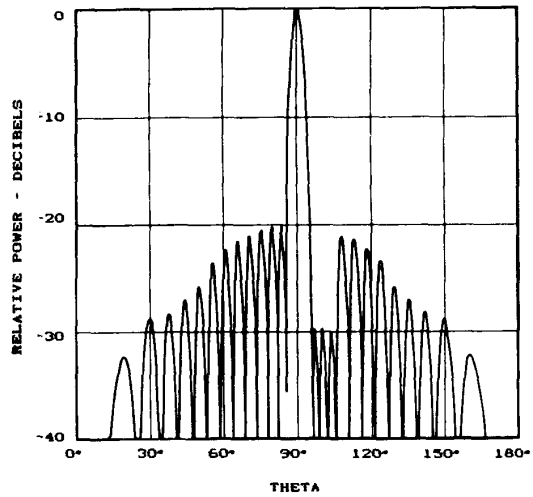

(a)

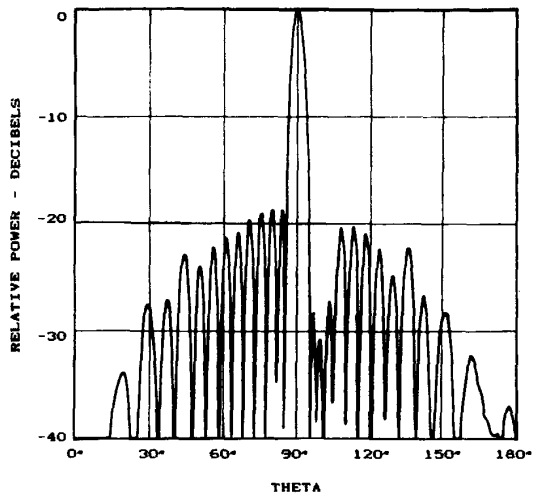

(b)

Fig. 15. Patterns for a Taylor distribution 20/20 modified with three 30-dB inner side lobes (from Elliott [21], [22]). (a) Computed pattern. (b) Pattern for 19-element X band longitudinal shunt slot array.

The sum becomes

$$A_a(u) = \sum a_n[\sin N\pi(u-n)]/N\sin\pi(u-n). \quad (24)$$

The composite phase and amplitude distribution is obtained by summing the excitations of all the arrays at the location of each element, resulting in a composite phase and amplitude distribution. Ripples in the pattern will occur because the side lobes of all the individual beams contribute between sample points as well as outside the shaped beam region. The ripple and drop-off slopes of the pattern will depend on the available aperture size, the number and spacing of the elements. Since the publication of Woodward's paper, several iterative techniques have been developed. In a recent technique [24], both the ripples on the shaped

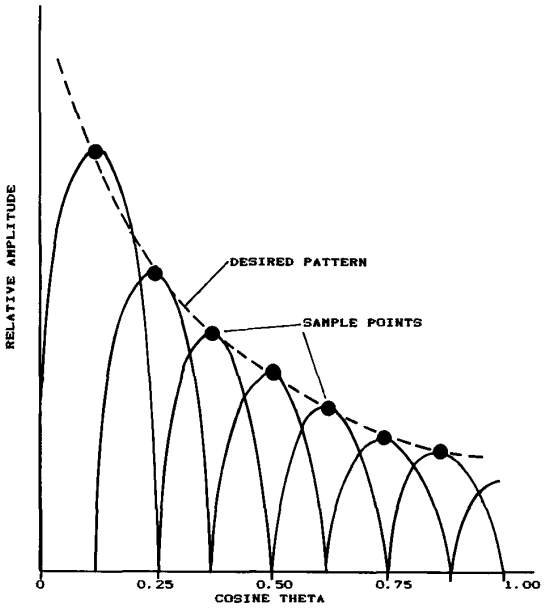

Fig. 16. Shaped beam pattern synthesis.

beam and the height of the side lobes are controlled. Roots outside the Schelkunoff unit circle represent minima in the ripples of the shaped beam. Iterations on the roots are used to obtain the desired patterns. Figure 17 shows both the computed and measured E plane patterns from a 15-GHz slot array. Design goals were ±2-dB ripples and side lobe fall-off that for a uniform array; the theoretical and experimental patterns show good correlation.

The full capability of an electronically steered antenna array is realized when both the phase and amplitude are controlled independently. This capability is used in adaptive arrays, with complex weights (equivalent to phase and amplitude controls) at each element, to steer pattern nulls toward jamming signals received from unknown angles of arrival [25]. In most cases, the phased array designer, however, is limited to the control of the element phases[6] and to an *a priori* amplitude taper. To extend the capability of phased arrays to include null steering, the sum (output) port is used to detect the jamming signals, the phase shifters are sequenced through the phase states to reduce the interference. The emphasis has been to develop programming for the phase shifters and robust algorithms that achieve convergence while the jammer/array geometry is stationary [28], [29].

VI. Conformal Arrays

Planar arrays are usually limited to scan angles of about ±70° from broadside because of gain reductions and aperture mismatch losses. Scanning beyond that angular range would require multiple apertures on multifaceted systems.

[6]Interestingly enough, beam scanning has also been accomplished by amplitude control alone [26], [27].

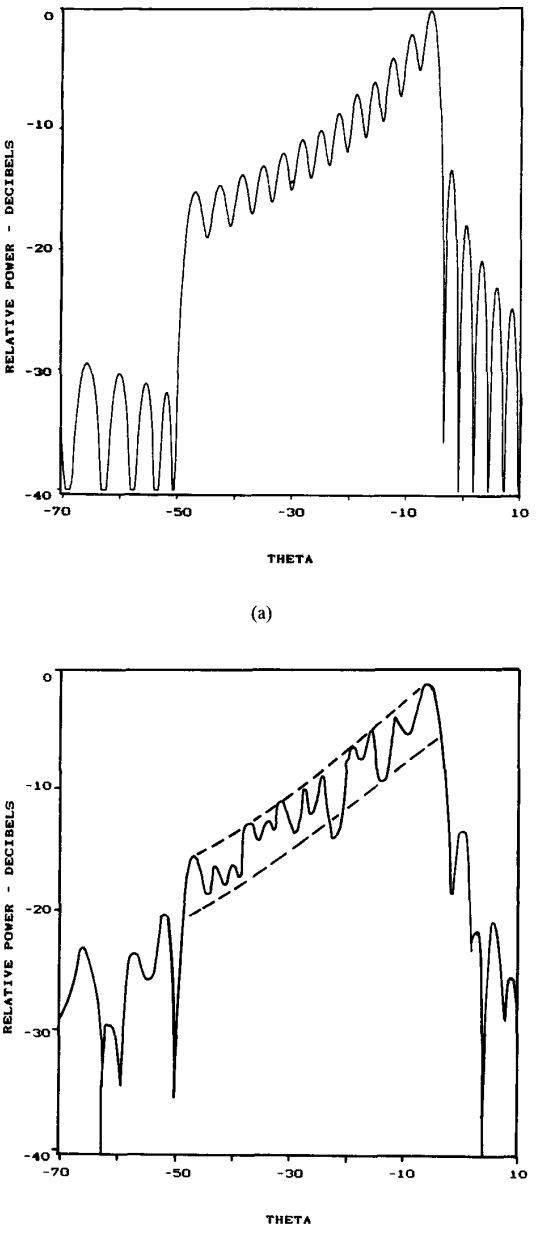

Fig. 17. E plane pattern for 6 by 26 slot array. (a) Computed pattern. (b) Measured pattern, Ku-band array (from Orchard [24]).

The alternative is the location of radiators on circularly symmetric surfaces, such as cylinders, cones or spheres [30]. Full circumferential scans may be accomplished by illuminating an arc or sector and then advancing that sector electronically to cover the 360° scan. An application for the extended scan would be in missiles and high speed aircraft, where the substitution of the dielectric radome with a metallic surface filled with flush-mounted radiators would have several advantages: no large radome, and thus no radome heating, ablation, boresight errors and side lobe

degradation.

Practical implementation problems of conformal arrays are significant and include element spacing, polarization matching, feeding systems, and beam steering.

Analysis of conformal arrays can be divided into three areas: 1) the analysis of active element patterns [31], 2) pattern analysis and synthesis that specify excitations on the surface, and 3) the problem of designing the radiators and the feed networks to obtain the desired excitations. Our focus will be on pattern synthesis.

One of the most challenging problems in conformal arrays is pattern synthesis. Most linear and planar array analysis is concerned with arrays large in terms of wavelength, for all practical purposes infinite in extent insofar as analysis of the radiating element is concerned. All elements are postulated identical in pattern, polarization, gain, orientation, and impedance. In conformal arrays, the patterns of the elements point in different directions, the element pattern cannot be factored out from the array pattern [32]. Figure 18 shows what may be an extreme example, a conical array with slots oriented to give linear polarization in the axial direction. Consequently, the usual synthesis techniques for planar arrays are not directly translatable to conformal arrays: there is no proven synthesis technique available. To illustrate how conformal arrays must be handled differently, let us examine an arc array where elements are located on an arc of a circle as in Fig. 19. The inputs to (4) are $x' = a\cos\phi', y' = a\sin\phi', z' = 0; x = \rho\cos\phi, y = \rho\sin\phi, z = 0$. The pattern is

$$A(\phi) = \sum_{n=-N}^{N} A_{en}(\phi - n\Delta)I_n \cdot \exp(jka\cos(\phi - n\Delta)). \quad (25)$$

In order to obtain in-phase addition of the elements (the "cophasal condition"), at $\phi = 0$, a feed network with appropriate phasing is provided. For purposes of analysis, this type of array is sometimes analyzed by projecting it on a plane perpendicular to the beam pointing direction. This resulting array is considered an equivalent linear array, with symmetrically placed, unequally spaced elements with each element pattern pointing in a different direction in space. In spite of the fact that the spacing is only 0.6 λ, a grating lobe not predicted by linear array theory appears, as shown in Fig. 20 [33]. This grating lobe appears around 100°, where the radiation of the last few elements tend to add in phase; most of the others are not visible from that direction.

To scan the beam of an arc array around 360°, the array is replicated around the periphery and the feed network is advanced electronically. Several examples are found in the literature [34], [35]. To obtain narrow or shaped beams in θ, linear arrays may be substituted for the radiating elements along the generatrices, creating a two-dimensional array, in this case a cylindrical array.

As was seen, the linear array techniques, as applied to the circular array, predict near-in side lobes, but not far-out grating lobes. Thus conventional planar array synthesis techniques are not adequate when applied to conformal

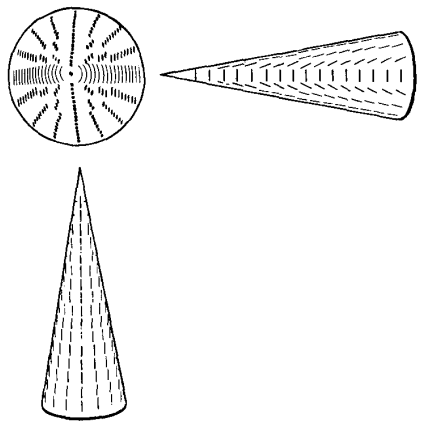

Fig. 18. Conical array, slots oriented for linear polarization in axial direction.

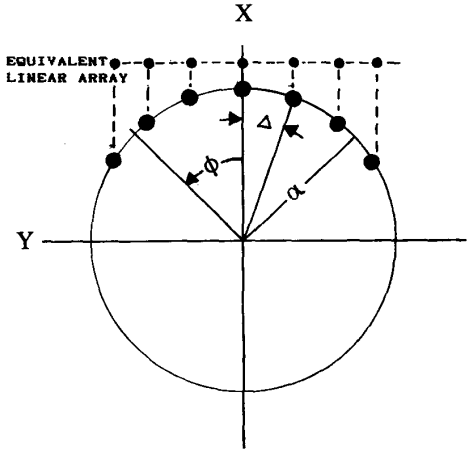

Fig. 19. Geometry for arc array.

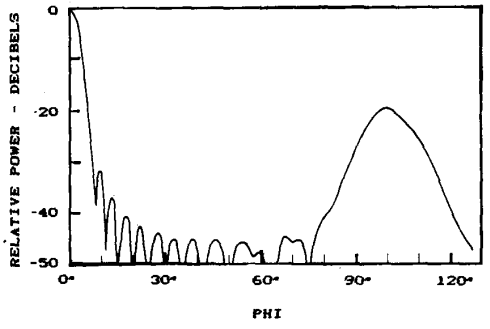

Fig. 20. Computed pattern of 25 Element Arc Array. Array radius 6.72λ; Element spacing 5.63°, 0.66λ; Array taper 23 dB; Element pattern cos (θ) in half-space; after Howard [33].

arrays. One possible approach to a pattern synthesis technique is the use of the equivalence principle [3]. The

complete fields generated by a fictitious planar array, whose aperture distribution is synthesized by known planar array techniques, is evaluated on the conformal surface. The fictitious aperture is contained entirely within the conformal surface. As an illustration, the technique will be applied to a conical surface; the method of approach will outlined below [36], [37].

A reference antenna, say a mechanically scanned planar array (Fig. 21), is the antenna whose pattern is desired from the excitations of the conical array. The excitations of the slots for the planar array are determined by the conventional design techniques; it is positioned to be entirely within the cone for all scan angles. The components of the electric fields tangential to the conformal surface are converted to magnetic source currents on the conducting surface, so that looking from the outside of the cone, the fields will be identical to that generated by the planar array.

In any practical situation, the required continuous magnetic current density can only be approximated by discrete magnetic sources distributed over the conical surface. Consequently, the resulting pattern from discrete magnetic

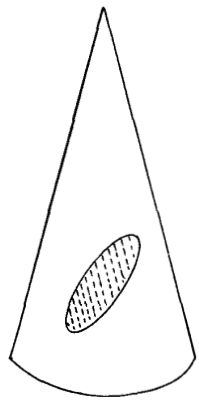

Fig. 21. Planar array located within conical surface.

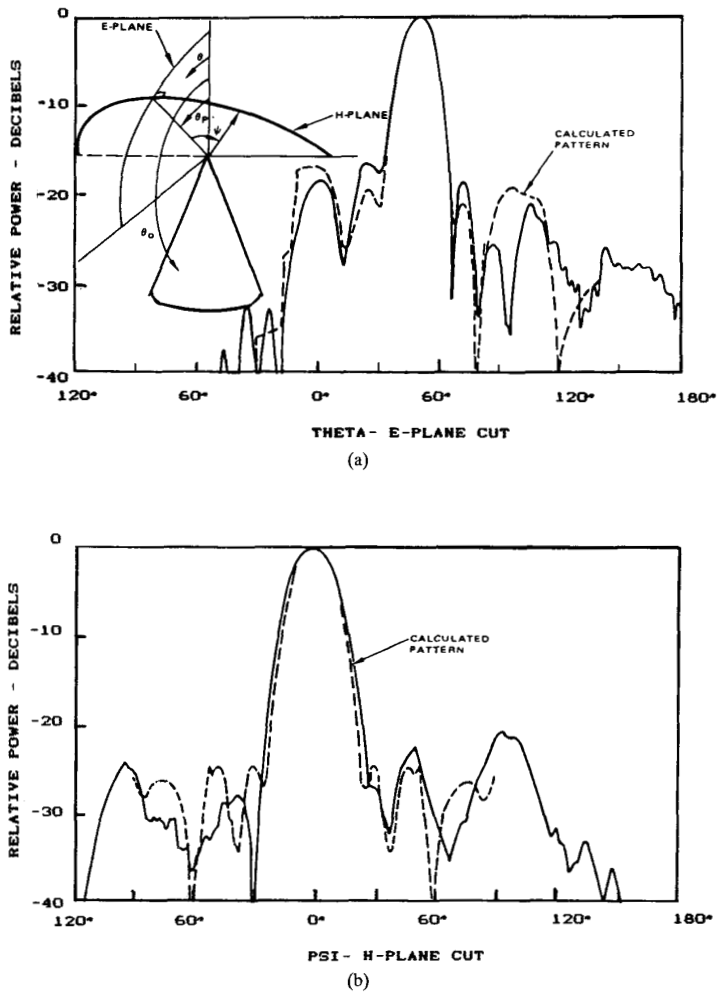

Fig. 22. Measured E and H plane patterns of conical array located 8.70λ from tip. Beam position at $\theta_P = 50°$, $\phi_P = 0°$; $\theta_0 = 169.75°$ (from Villeneuve [36]).

sources will deviate from the desired pattern. The amount of deviation will depend on the spacing of the sources on the cone. This spacing should be as large as practical while still providing an acceptable pattern.

The computer mechanization of the synthesis technique approximates the pattern of the reference planar array of slot radiators by replacing the planar array by an array of crossed slots with independently excited arms on the conical surface. The radiation pattern of each slot is represented by a simple approximate expression that does not include tip diffraction.

An experimental array of 37 crossed slot radiators was designed, fabricated, and tested. It had a 20.5° full cone angle with a stripline feed network for controlling the phases and amplitudes of the radiating elements. Excitations were adjusted to the one predicted by the theory. Comparison between experiment and theory shows good agreement (Fig. 22). The sharp cutoffs in the theoretical patterns are due to approximate element patterns used in the theory. Measured cross-polarization was less than 25 dB in the E plane and 20 dB in the H plane.

ACKNOWLEDGMENT

The author would like to acknowledge the helpful suggestions made by the reviewers. Special thanks go to Dr. Winifred E. Kummer and to Dr. A. T. Villeneuve for their critical review of the paper.

REFERENCES

[1] Y. T. Lo, "Aperiodic arrays," in *Antenna Handbook,* Y. T. Lo and S. W. Lee, Eds. New York: Van Nostrand Reinhold, 1988, pp. 14-1–14-37, ch. 14.
[2] M. I. Skolnik, "Nonuniform arrays," in *Antenna Theory,* R. E. Collin and F. J. Zucker, Eds. New York: McGraw-Hill, 1969, pp. 207–227, pt. 1, ch. 6.
[3] R. F. Harrington, *Time Harmonic Electromagnetic Fields.* New York: McGraw-Hill, 1961, pp. 106–134, ch. 3.
[4] R. S. Elliott, "The theory of antenna arrays," in *Microwave Scanning Antennas,* R. C. Hansen, Ed. New York: Academic, 1965; Los Altos, CA: Peninsula, 1985, pp. 9–53, vol. II, ch. 1.
[5] S. A. Schelkunoff, "A mathematical theory of linear arrays," *Bell Syst. Tech. J.,* vol. 22, pp. 80–107, Jan. 1943.
[6] R. S. Elliott, *Antenna Theory and Design.* Englewood Cliffs, NJ: Prentice-Hall, 1981, pp. 128–193, ch. 4, 5.
[7] C. L. Dolph, "A current distribution for broadside arrays which optimizes the relationship between beamwidth and side lobe level," *Proc. IRE,* vol. 34, pp. 335–348, 1946.
[8] A. T. Villeneuve, "Taylor patterns for discrete arrays," *IEEE Trans. Antennas Propagat.,* vol. AP-32, pp. 1089–1093, Oct. 1984.
[9] T. T. Taylor, "Design of line-source antennas for narrow beamwidth and low sidelobes, *IRE Trans. Antennas Propagat.,* vol. AP-7, pp. 16–28, Jan. 1955.
[10] R. C. Hansen, "Aperture theory," in *Microwave Scanning Antennas,* R. C. Hansen, Ed. New York: Academic, 1965; Los Altos, CA: Peninsula, 1985, pp. 47–105, vol. I, ch. 1.
[11] W.L Stutzman and G. A. Thiele, *Antenna Theory and Design.* New York: Wiley, 1981, pp. 141–145, ch. 3.
[12] F. I. Tseng and D. K. Cheng, "Optimum scannable planar arrays with an invariant sidelobe level," *Proc. IEEE,* vol. 56, pp. 1771–1778, Nov. 1968.
[13] L. Stark, "Microwave theory of phased-array antennas—A review," *Proc. IEEE,* vol. 62, pp. 1661–1701, Dec. 1974.
[14] W. H. Von Aulock, "Properties of phased arrays," *Proc. IRE,* vol. 48, pp. 1715–1727, Oct. 1960.
[15] E. D. Sharp, "A triangular arrangement of planar-array elements that reduces the number needed", *IEEE Trans. Antennas Propagat.,* vol. AP-9, pp. 126–129, Mar. 1961.
[16] R. J. Mailloux, "Antenna array architecture," *Proc. IEEE,* vol. 80, this issue.
[17] R. C. Hansen, "Linear arrays," in *The Handbook of Antenna Design,* A. W. Rudge *et al.,* Eds. London, UK: Peregrinus, 1983, pp. 104–109, vol. 2, ch. 9.
[18] R. Tang, "Array technology," *Proc. IEEE,* vol. 80, this issue.
[19] C. J. Miller, "Minimizing the effects of phase quantization errors in an electronically scanned array," in *Proc. 1964 Symp. Electronically Scanned Array Techniques and Applications,* 1964, pp. 17–38, vol. 1.
[20] T. C. Cheston and J. Frank, "Array antennas," in *Radar Handbook,* M. I. Skolnik, Ed. New York: McGraw-Hill, 1970, pp. 11-35–11-43, ch. 11.
[21] R. S. Elliott, "Design of line-source antennas for sum patterns with sidelobes of individually arbitrary heights," *IEEE Trans. Antennas Propagat.,* vol. AP-24, pp. 76–83, Jan. 1976.
[22] R. S. Elliott and R. M. Johnson, "Experimental results on a linear array designed for asymmetric sidelobes," *IEEE Trans. Antennas Propagat.,* vol. AP-26, pp. 351–352, Mar. 1978.
[23] P. M. Woodward, "A method of calculating the field over a plane aperture required to produce a given polar diagram," *Proc. Inst. Elect. Eng.,* pp. 1554–1558, 1947.
[24] H. J. Orchard, R. S. Elliott, and J. J. Stern, "Optimising the synthesis of shaped beam antenna patterns," *Proc. Inst. Elect. Eng.,* vol. 123, pt. H, pp. 63–68, Feb. 1985.
[25] W. F. Gabriel, "Adaptive Processing Array Systems," *Proc. IEEE,* vol. 80, this issue.
[26] C. J. Sletten, P. Blacksmith, and L. F. Shodin, "Amplitude scanning of antenna arrays," AFCR-TR-58–124, (ASTIA Doc. AD146899), Mar. 1958.
[27] J. P. Costas, "An antenna beam steering technique comprised of constant-phase array elements," *Proc. IEEE,* vol. 69, pp. 745–746, June 1981.
[28] P. A. Thompson, "Adaptation by direct phase-shift adjustment in narrow-band adaptive antenna systems," *IEEE Trans. Antennas Propagat.,* vol. AP-24, pp. 756–760, Sept. 1976.
[29] T. S. Fong, "An interference nulling algorithm for a single receiver phased array", *IEEE Trans. Antennas Propagat.,* vol. 38, pp. 951–953, June 1990.
[30] R. J. Mailloux, "Conformal and low-profile arrays," in *Antenna Engineering Handbook,* R. C. Johnson, H. Jasik, Eds. New York: MacGraw-Hill, 1981, pp. 21-1–21-21, ch. 21.
[31] G. V. Borgiotti, "Conformal arrays," in *The Handbook of Antenna Design,* A. W. Rudge *et al.,* Eds. London, U.K.: Peregrinus, 1983, pp. 227–297, vol. 2, ch. 11.
[32] W. H. Kummer, "Preface, Special Issue on conformal arrays," *IEEE Trans Antennas Propagat.,* vol. AP-22, pp. 1–3, Jan. 1974.
[33] J. E. Howard, "Statistical patterns of a general array," *IEEE Trans Antennas Propagat.,* vol. AP-15, pp. 60–65, Jan. 1967.
[34] Special Issue, "Conformal arrays," *IEEE Trans. Antennas Propagat.,* vol. AP-22, Jan. 1974.
[35] W. H. Kummer, "Broad-band microwave electronically scanned direction finder," *IEEE Trans. Antennas Propagat.,* vol AP-31, pp. 18–26, Jan. 1983.
[36] A. T. Villeneuve, in *Conformal Antenna Array Design Handbook,* Dep. of the Navy, ASC, Doc. AD-A1110091, pp. 145–192, Sept. 1981.
[37] A. T. Villeneuve *et al.,* "Conical phased array antenna investigations," Final Rep., Hughes Aircraft, Culver City, CA, Contract N000191&–77-C-0358, Apr. 1979.

Wolfgang H. Kummer (Life Fellow, IEEE) received the B.S. (Honors), M.S., and the Ph.D. degrees from the University of California, Berkeley, in 1946, 1947, and 1954, respectively.

While at the University of California he was Lecturer in electrical engineering and a Research Engineer with the Electronics Research Laboratory. In 1953 he joined the Radio Research Department, Bell Telephone Laboratories, Holmdel, NJ, where he performed research in the fields of antennas and radio-wave propa-

gation, including tropospheric propagation beyond-the-horizon. From 1959 to 1985 he was with the Hughes Aircraft Company, Culver City, CA, and became Chief Scientist of the Antenna Systems Laboratory, Radar Systems Group. His responsibilities included the formulation, direction, and management of advanced antenna and radio propagation programs. These included work on signal processing antennas, adaptive arrays, satellite antenna systems, conformal arrays, millimeter-wave propagation and radar systems, multibeam, and phased arrays. He holds three patents on phased array antenna systems. He is currently a consultant specializing in antenna systems and radio-wave propagation. He also has been lecturer at the University of California, Los Angeles, California State University, Northridge, and at the University of Southern California.

Dr. Kummer is a member of US URSI Commissions A and F, Sigma Xi, Phi Beta Kappa, Tau Beta Pi, and Eta Kappa Nu. He was Editor of the GAP Newsletter (1964–1968), General Chairman of the 1971 GAP International Symposium and URSI Fall Meeting, President of the APS AdCom (1975), and Chairman of Standards Subcommittee 2.11 that revised the Standard on Test Procedures on Antennas.